Temperature-Dependent Elasticity of a Semicrystalline Interphase Composed of Freely Rotating Chains

Pieter J. in 't Veld and Gregory C. Rutledge*

Department of Chemical Engineering, Massachusetts Institute of Technology, Cambridge, Massachusetts 02139

Received May 20, 2003; Revised Manuscript Received July 23, 2003

ABSTRACT: We describe a method for determining the thermal and elastic properties of the noncrystalline phase of semicrystalline polymers (the "interphase") by Monte Carlo simulations. The method is applied to an interphase composed of freely rotating polyethylene-like chains, studied previously by Balijepalli and Rutledge (*J. Chem. Phys.* **1998**, *109*, 6523). The isochoric and isobaric heat capacities, Grüneisen coefficients, thermal expansion coefficients, and elastic stiffnesses are reported. The interphase exhibits material properties comparable to that of the corresponding melt, with significant contributions of both enthalpic and entropic origins. Through judicious selection of Monte Carlo moves, we approximate the rate sensitivity of the stiffness normal to the crystal surface, C_{33}, on time scales that are long and short, respectively, relative to the characteristic time scale of the crystalline α_c relaxation.

1. Introduction

Crystallizable polymers are typically only semicrystalline in the solid state. A wide range of morphologies composed of crystalline and noncrystalline domains are possible, depending on material and processing conditions. Typical morphologies are spherulitic and transcrystalline, as well as other morphologies achieved under special processing conditions. As a consequence of their two-component nature, the properties of such materials are characterized by the behavior of both the crystalline fraction and the constrained amorphous material that is located between the crystal lamellae and intimately connected to them. However, experimental efforts to decouple these in such a way as to describe, respectively, the crystalline and noncrystalline responses have been complicated by the complexity of the experimentally available morphologies. One attempt to do so was reported by Al-Hussein et al.[1]

Alternatively, theoretical estimates of the behavior of the individual components of a semicrystalline material can be made by molecular modeling. Estimation of the thermoelastic properties of numerous polymeric crystals has been performed using quantum mechanics,[2,3] molecular dynamics,[4,5] Monte Carlo,[6] and lattice dynamics.[7,8] Elastic properties of the noncrystalline interlamellar domain, on the other hand, have eluded description. Monte Carlo molecular simulations of the interlamellar domain were reported for the first time by Balijepali and Rutledge.[9−11] The resulting "loop surfaces" arise as the natural consequence of a balance between entropically driven disordering throughout much of the interphase, and enthalpically favored packing of certain preferred short loops. From profiles of density and order, an interfacial thickness of approximately 1.0 nm was estimated for an interphase composed of free-rotating chains at 450 K. Subsequent simulations[12] showed that the [201]-oriented lamellar interface is energetically favored over other orientations, in accord with experimental observations.[13] In this article, we report theoretical estimates for the thermoelastic properties of the interlamellar domain, obtained by this Monte Carlo approach.

These simulations are based on an explicit definition of the criteria for metastability of the interlamellar domain. Molecular simulation of the noncrystalline domain of semicrystalline polymers depends on appropriate identification of the constraints, $W(p^N, q^N)$ operative on the metastable state. The partition function of a metastable state may be written[14] (in canonical form),

$$Q(N, V, T) = \int \dots \int \mathrm{d}p^N \, \mathrm{d}q^N \exp(-\beta E(p^N, q^N)) \exp(-\beta W(p^N, q^N)) \quad (1)$$

where p and q are momenta and coordinates, respectively, of the N atoms composing the molecular system, $E(p^N, q^N)$ is the internal energy, and the integration is performed over all of phase space. The constraint function $W(p^N, q^N)$ may vary from one metastable situation to another, or from polymer to polymer, just as $E(p^N, q^N)$ does, or even from sample to sample, depending on the history of the sample. However, one can anticipate that there are more or less general forms of $W(p^N, q^N)$, which are transferable in much the same way as $E(p^N, q^N)$.

As a first step, we have proposed that the constraints imposed on the noncrystalline phase in a polymer such as polyethylene are those due to the long-lived structure of the crystalline lamellae and the density of the noncrystalline domain.[9] Formally, one can write

$$W(p^N, q^N) = k_m\{\sum_{i=1}^{n_c<N} [1 - \delta(q_i - q_{i,hkl})] + [1 - \delta(\rho - f\rho_c)]\} \quad (2)$$

where n_c is the set of atoms at the boundary of the noncrystalline domain which are constrained to lie in crystallographic locations specified by the crystallographic facet (denoted by Miller indices h, k, and l) parallel to the lamellar surface, and ρ_c is the density of the crystal phase. f is a value other than 1. ρ is the average density of the noncrystalline domain; the local density may of course vary from one location to another

* Corresponding author.

10.1021/ma0346658 CCC: $25.00
Published on Web 08/23/2003

within the noncrystalline domain. The first constraint on the coordinates of the n_c atoms ensures that crystallographic order is preserved at some distance from the centerline of the interlamellar domain, so that the system cannot completely melt, even for temperatures above the melt temperature. This constraint is similar to that realized by earlier lattice simulations.[15] More importantly, the second constraint ensures that the interlamellar material does not crystallize throughout its volume when the temperature is below the crystallization temperature. Prior lattice simulations with fully occupied lattices were not subject to this constraint and hence should crystallize if they were below their crystallization temperature. k_m modulates the strength of the metastability constraints. In the Monte Carlo simulations reported here, the initial structure as well as the subsequent collection of allowed Monte Carlo moves were chosen so that the constraints required by eq 1 are never violated; k_m is effectively infinite.

2. Method

2.1. Force Field. The united atom model of Paul et al.,[16] with the exclusion of torsion angle terms, serves as a starting point in the description of freely rotating polyethylene-like chains. A Lennard-Jones potential is used to compute the nonbonded CH_2 interactions between all united atom pairs on different chain segments and those separated by four or more bonds in the same chain segment.

$$E_{\mathrm{LJ},ij} = 4\epsilon_{\mathrm{LJ}}\left[\left(\frac{\sigma_{\mathrm{LJ}}}{d_{ij}}\right)^{12} - \left(\frac{\sigma_{\mathrm{LJ}}}{d_{ij}}\right)^{6}\right], \quad d_{ij} = |\Delta\mathbf{r}_{ij}|, \quad \Delta\mathbf{r}_{ij} = \mathbf{r}_i - \mathbf{r}_j \tag{3}$$

where $\epsilon_{\mathrm{LJ}} = 390.95$ J/mol and $\sigma_{\mathrm{LJ}} = 0.4009$ nm; $\mathbf{r}_i$ and $\mathbf{r}_j$ represent the Cartesian coordinates of sites i and j respectively. Nonbonded interactions are truncated at a cutoff distance $r_c = 2.5\ \sigma_{\mathrm{LJ}}$. To this we have added a harmonic spring model for bond stretching (Bolton et al.[17])

$$E_{\mathrm{l},i} = \frac{1}{2}k_{\mathrm{l}}(l_i - l_0)^2 \tag{4}$$

where l_i is the length of bond i; the bond stretching constants are $k_{\mathrm{l}} = 37.61$ kJ/mol/nm^2 and $l_0 = 0.1530$ nm. Paul et al.[16] report the angle bending potential as a harmonic in cos θ. As an aside, we note that this differs from other reports by them and by others, which are harmonic in θ.[17−20] To correct for this, we use the form employed by Paul et al., but with a stiffness constant given by $k_\theta/\sin^2\theta_0$

$$E_{\theta,i} = \frac{1}{2}\frac{k_\theta}{\sin^2\theta_0}(\cos\theta_i - \cos\theta_0)^2 \tag{5}$$

which is obtained from the first term of a Taylor series expansion about θ_0 of a potential harmonic in cosθ. The angle bending constants are $k_\theta = 502.1$ kJ/mol and $\theta_0 = 68.0°$, the bond angle complement.

2.2. Simulation Method. The Monte Carlo simulations were performed in the (N, n, V, T, μ_i^*) ensemble, in which the total number of chain segments (N), total number of sites (n), volume (V), and temperature (T) of the simulation were fixed. For chain segments of different lengths, the chemical potential per site was also assumed to be constant (i.e., reduced chemical potential $\mu_i^* = 0$), as suggested by Kumar et al.[21] Chain segments may be loops, bridges or tails, according to their topological connectivity to the crystal lamellae. Five types of Monte Carlo moves were applied to sample configuration space; these serve to change both the local conformation of the chains and the topology of the interphase. The first four, end-rotation,[10] reptation,[22,23] concerted rotation[24] (also known as "intramolecular rebridging"[25]), and site displacement moves, sample changes in conformation and local packing. The end-rotation move performs a simple rotation of one to three sites at the free end of a tail. The reptation move removes a segment from the end of one tail and appends it to the end of another tail with a randomly selected torsion angle. The rebridging move, first developed by Dodd et al.[24] and later mathematically refined by Mavrantzas et al.,[25] excises three consecutive sites in a chain and solves for all the possibilities by which these sites can be reinserted in the chain without changing bond lengths or angles. One of these solutions is then chosen at random for the Monte Carlo attempt. If accepted, the concerted rotation move results in a change of 6 torsional degrees of freedom. The site displacement move simply translates a molecular site a small distance in Cartesian coordinates, thereby altering bond lengths and angles. This move was not used in previously reported interphase simulations; it is important in this work, however, where deformation of taut bridge molecules can occur. The fifth move, end-bridging,[26] samples both conformational and topological spaces. The end-bridging move, or a similar move that alters the connectivity of chains, such as double bridging,[10,27] is essential to obtain an unbiased sample of interfacial topologies during a simulation. In end-bridging, the end of one segment (a tail) "attacks" a set of three united atoms in a nearby segment (a loop or bridge). Solutions for placement of the three atoms are such that the tail and part of the original loop (or bridge) become a new segment, and the remaining atoms of the loop (or bridge) form a new tail. The end-bridging move was optimized by prescreening for all mathematically feasible solutions, as described in Appendix B of Mavrantzas et al.,[25] before entering the energetic acceptance phase. During equilibration and simulation, each of the five moves was chosen with equal probability.

A parallel tempering scheme was used to efficiently sample the temperature dependence of the simulated quantities and to enhance the sampling of the lower temperature states. Parallel tempering promotes more efficient sampling of lower temperature states by exchange with more mobile higher temperature states. It has the added benefit of generating properties over a range of temperatures, from which the temperature dependence of the investigated properties can be obtained. The spacing between the different temperatures is chosen to ensure at least a 30−40% acceptance rate for swapping two adjacent temperature configurations.[28]

2.3. Virial Calculation of Stress. The instantaneous stress tensor σ_{ij} resulting from the interaction of site i with site j is computed by using the atomic virial tensor $\mathbf{W}_{ij}$,

$$\sigma_{ij} = -\frac{\mathbf{W}_{ij}}{V} = \frac{1}{V}\mathbf{r}_i{}^{\mathrm{t}}\nabla_j E \tag{6}$$

where V represents the system volume, ∇_j indicates

differentiation with respect to displacement of site j, considering all other sites fixed, and superscript t denotes the vector transpose. The chain rule is used to compute contributions from bond lengths and angles, y_k

$$\nabla_j E = \sum_{\text{degrees of freedom}} \frac{\partial E}{\partial y_k} \nabla_j y_k \tag{7}$$

where k is summed over all the internal degrees of freedom used to parametrize the several contributions to the energy. The total instantaneous stress tensor σ is found by adding its separate Lennard-Jones, bond angle, and bond length contributions

$$\sigma = -\frac{1}{V}\Big(\sum_{i=1}^{N_{\text{sites}}-1}\sum_{j>i}^{N_{\text{sites}}} \mathbf{W}_{\text{LJ},ij} + \sum_{i=1}^{N_l}\mathbf{W}_{l,i} + \sum_{i=1}^{N_\theta}\mathbf{W}_{\theta,i} + \mathbf{W}_{\text{ideal}}\Big),\ \mathbf{W}_{\text{ideal}} = N_{\text{sites}} k_B T\, \mathbf{I} \tag{8}$$

where V is the volume of the simulation box, N_{sites} is the number of sites, N_l is the number of bonds, N_θ is the number of bond angles, $\mathbf{W}_{\text{ideal}}$ is the ideal gas contribution, k_B is the Boltzmann constant, and $\mathbf{I}$ is the unit matrix. Crystal−crystal interactions are excluded. The Lennard-Jones contribution to the virial tensor $\mathbf{W}_{\text{LJ},ij}$ for each pair of atoms i and j is[29]

$$\begin{aligned}\mathbf{W}_{\text{LJ},ij} &= -\Delta\mathbf{r}_{ij}{}^{\text{t}}\nabla_j E_{\text{LJ},ij} \\ &= 24\epsilon_{\text{LJ}}\left[2\left(\frac{\sigma_{\text{LJ}}}{d_{ij}}\right)^6 - 1\right]\left(\frac{\sigma_{\text{LJ}}}{d_{ij}}\right)^6 \frac{\Delta\mathbf{r}_{ij}{}^{\text{t}}\Delta\mathbf{r}_{ij}}{d_{ij}}\end{aligned} \tag{9}$$

The same summation rules apply to the Lennard-Jones virial tensor as do for the Lennard-Jones energy. As a result of Lennard-Jones potential truncation, a long-range correction $w_{\text{LJ},ij}$ is added to $\mathbf{W}_{\text{LJ},ij}$,

$$w_{\text{LJ},ij} = \frac{16\pi\epsilon_{\text{LJ}}\sigma_{\text{LJ}}{}^3}{9V_0}\left(\frac{\sigma_{\text{LJ}}}{r_c}\right)^3\left[2\left(\frac{\sigma_{\text{LJ}}}{r_c}\right)^6 - 3\right] \tag{10}$$

The bond stretch contribution to the virial tensor $\mathbf{W}_{l,i}$ for bond i is

$$\mathbf{W}_{l,i} = -k_l\frac{l_i - l_0}{l_i}\Delta\mathbf{r}_i{}^{\text{t}}\Delta\mathbf{r}_i \tag{11}$$

with $\Delta\mathbf{r}_i$ as the bond vector of bond i. The bond angle contribution to the virial tensor $\mathbf{W}_{\theta,i}$ for angle θ_i is

$$\mathbf{W}_{\theta,i} = -\frac{k_\theta}{\sin^2\theta_0}(\cos\theta_i - \cos\theta_0)(\Delta\mathbf{r}_{i-1}{}^{\text{t}}\mathbf{g}_{-1} + \Delta\mathbf{r}_i{}^{\text{t}}\mathbf{g}_0) \tag{12}$$

where

$$\begin{aligned}\mathbf{g}_{-1} &= \frac{1}{l_{i-1}}\left(\frac{\Delta\mathbf{r}_i}{l_i} - \cos\theta_i\frac{\Delta\mathbf{r}_{i-1}}{l_{i-1}}\right) \\ \mathbf{g}_0 &= \frac{1}{l_i}\left(\frac{\Delta\mathbf{r}_{i-1}}{l_{i-1}} - \cos\theta_i\frac{\Delta\mathbf{r}_i}{l_i}\right),\end{aligned} \tag{13}$$

also with $\Delta\mathbf{r}_i$ as the bond vector of bond i. The trace of the instantaneous contributions to $\mathbf{W}_{\theta,i}$ is mathematically zero as was shown independently by Honell et al.[30] and Theodorou et al.[31] We observe that off-diagonal total stresses average to zero in the absence of externally applied shear stresses.

2.4. Initial Configurations. Initial configurations were generated by building a model of the polyethylene crystal with dimensions 3a by 4b by 25c (ie. 2.22 nm by 1.96 nm by 6.35 nm), where $a = 0.74$ nm, $b = 0.49$ nm, and $c = 0.254$ nm are the dimensions of the crystallographic unit cell. The total cell volume for the unstrained configuration, V_0, is 27.6 nm^3. Each chain has a setting angle of ± 42°, in accord with experimental data on polyethylene. To simulate the crystal boundary constraints and to provide a layer of united atoms thick enough to include all nonbonded interactions between noncrystalline and crystalline layers up to the cutoff distance r_c, the five united atom sites at either end of each chain segment in the initial structure are permanently fixed. This corresponds to the [001]-oriented interface. Next, a total of 114 sites are deleted from 6 randomly selected chains; the remaining segments are terminated in end sites, to form tails. The final simulation cell has 1086 sites distributed into 30 chain segments, of which 12 chains are tails and 18 chains are taut bridges extending from one crystal boundary to the other. The resulting density of the noncrystalline portion of the cell, i.e., the part excluding the regimes containing the fixed 5-site segments, is 0.890 g/cm^3, which after equilibration is distributed inhomogeneously through the cell. Because the density of sites at the interface is unknown prior to simulation, this density was determined by trial and error in order to ensure an amorphous phase density of 0.85 g/cm^3 at the centerline of the cell, the density of an amorphous polyethylene melt extrapolated to 300 K.[32] The fraction of end groups and the fraction of sites where chains enter a crystal boundary in the simulation govern the molecular weight of the polymer sample.[33] In this work, the corresponding molecular weight is roughly 9000 g/mol for polyethylene. During simulation, the combined number of bridges and loops, and the number of tails, do not vary. However, the lengths of segments in each population are free to vary, as are the number of either bridges or loops. Ten structures with identical volume and number of sites are thus created. The final structures are randomized at 10 000 K for 100 cycles, followed by a quench to a temperature range of 350−462.5 K with steps of $\Delta T = 12.5$ K. Decay studies of the energy autocorrelation function confirm equilibration in 25 000 cycles. One cycle consists of 1086 Monte Carlo trial moves. The equilibrated configurations function as a starting point for mechanical property simulations. All simulations were run for 100 000 cycles. Swaps between temperatures were attempted every 5 cycles.

2.5. Thermal and Elastic Properties. Thermal properties for the interphase are determined from least-squares fits of internal energy and stress, respectively, to an equation of the form

$$f = f_0 + \left[\frac{\partial f}{\partial T}\right]_0 \Delta T + \left[\frac{\partial^2 f}{\partial T^2}\right]_0 \Delta T^2 \tag{14}$$

When $f = \sigma_i$, we obtain $(\partial\sigma_i/\partial T)_0$ which, by a Maxwell relation, is equal to $(\partial S/V_0\partial\epsilon_i)_0$. When $f = E$, we obtain the isochoric heat capacity, $C_v = (\partial E/\partial T)_0$. We include the kinetic energy contribution to E. Using these two

pieces of information, we determine the Grüneisen coefficients, γ_i

$$\gamma_i = -\frac{V_0}{C_v}\left[\frac{\partial \sigma_i}{\partial T}\right]_0 \tag{15}$$

Temperature dependences of C_v and γ_i are obtained from the second-order term in eq 14. Using Voigt or matrix notation, the elastic stiffness moduli C_{ij} are defined as[34]

$$\sigma_i = \sum_{j=1}^{6} C_{ij}\,\epsilon_j$$

$$C_{ij} = \left[\frac{\partial \sigma_i}{\partial \epsilon_j}\right] \tag{16}$$

where σ_i is the i component of the stress, and ϵ_j is the j component of the strain. The isothermal stiffness modulus C_{ij}^{T} can be defined as

$$C_{ij}^{\mathrm{T}} = \frac{1}{V_0}\left[\frac{\partial^2 A}{\partial \epsilon_i \partial \epsilon_j}\right]_{\mathrm{T},\epsilon_{k\neq i,j}}$$

$$= \frac{1}{V_0}\left[\frac{\partial^2 E}{\partial \epsilon_i \partial \epsilon_j}\right]_{\mathrm{T},\epsilon_{k\neq i,j}} - \frac{T}{V_0}\left[\frac{\partial^2 S}{\partial \epsilon_i \partial \epsilon_j}\right]_{\mathrm{T},\epsilon_{k\neq i,j}} \tag{17}$$

where A is the Helmholtz free energy, E is the internal energy, S is the entropy, V_0 is the unstrained volume, and subscript T indicates isothermal conditions. It is possible in some instances[35,36] to show that the second term on the right-hand side of eq 17 is negligible, based on thermodynamic arguments. The validity of this assumption can also be checked directly by use of a virial calculation of the stress,

$$\sigma_i = \frac{1}{V_0}\left[\frac{\partial A}{\partial \epsilon_i}\right]_{\mathrm{T},\epsilon_{k\neq i}} = \sigma_i^{\mathrm{int}} - \frac{\gamma_i\, T\, C_v}{V_0} \tag{18}$$

where

$$\sigma_i^{\mathrm{int}} = \frac{1}{V_0}\left[\frac{\partial E}{\partial \epsilon_i}\right]_{\mathrm{T},\epsilon_{k\neq i}} \tag{19}$$

and use has been made of the Maxwell relationship between entropy S and stress. To estimate the magnitude of these derivatives, simulations were performed wherein the simulation box was held at a constant strain, and the internal energy and virial stress were calculated. Strains of ± 0.025 and ± 0.05 were imposed in the x, y, and z directions individually, and strains of ± 0.013 and ± 0.025 were imposed pairwise in (x, y), (x, z), and (y, z) directions. For this model system of freely rotating chains, no shear deformations were performed, our primary aim being only to demonstrate the method. United atoms which composed fixed segments of chains in the crystal boundary were displaced affinely as rigid segments, while united atoms which composed flexible segments of the chains within the body of the simulation cell were displaced affinely as individual atoms. The simulation cell was then reequilibrated at the new strain using the usual Monte Carlo moves. In this way, 25 data points (four states of strain in each of six modes of deformation, plus the reference state) were obtained for stress and energy. Using parallel tempering, all deformations were performed at 10 temperatures ranging from 350 to 462.5 K simultaneously. Error bars were estimated by dividing each simulation into 20 blocks and using block averaging.[37]

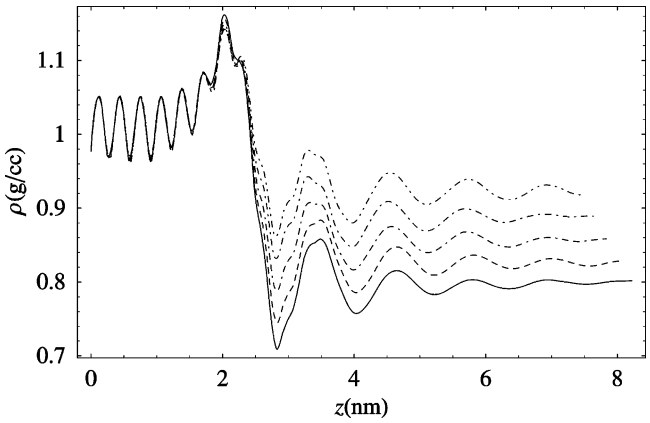

Figure 1. Density profiles for deformations normal to the [001] interface at 350 K, $\epsilon_3 \in \{-0.025, -0.013, 0.000, 0.013, 0.025\}$ in order from top curve (dot−dot−dash) to bottom curve (solid).

The deformation results for internal energy and stress were each approximated by a least squares fit to a Taylor series expansion around the unstrained state − denoted by subscript 0

$$f = f_0 + \sum_{i=1}^{3}\epsilon_i\left(\left[\frac{\partial f}{\partial \epsilon_i}\right]_{\mathrm{T},\epsilon_{k\neq i}}\Bigg|_0 + \frac{1}{2}\sum_{j=1}^{3}\epsilon_j\left[\frac{\partial^2 f}{\partial \epsilon_i \partial \epsilon_j}\right]_{\mathrm{T},\epsilon_{k\neq i,j}}\Bigg|_0\right) \tag{20}$$

When $f = \sigma_k$, $k = 1, 2, 3$, elastic stiffnesses are estimated from the first-order term, $\partial\sigma_k/\partial\epsilon_i$. The second-order term, $\partial^2\sigma_k/\partial\epsilon_k\partial\epsilon_j$ yields a measure of deviation from linear elasticity. Taking the ratio of the second term in the parentheses in eq 20 to the first term in the parentheses indicates about 15% of the energy of deformation is due to nonlinear elasticity for the range of strains used in this work. When $f = E/V_0$, the internal energy density, the first-order term in the fit yields an estimate of the internal energy component of stress, $\sigma_i^{\mathrm{int}} = 1/V_0\ \partial E/\partial\epsilon_i$ while the second-order term yields the internal energy contribution to elastic stiffness, $C_{ij}^{\mathrm{int}} = (1/V_0)\partial^2 E/\partial\epsilon_i\partial\epsilon_j$ (cf. eq 17).

3. Results and Discussion

3.1. Temperature and Density Dependence of the Interfacial Structure. Profiles in density and orientational order over the range of temperatures and strains studied were plotted and compared to those obtained previously for the [001]-oriented interface for the freely rotating polyethylene-like chain at 450 K. The density is computed as a function of distance from the crystal boundary in the simulation and normalized by the crystal density. Figure 1 shows the variation in the density profile at 350 K for several strains. Each strain is equivalent to an interphase simulated at a different density. For the range of strains shown, the density of the noncrystalline portion of the cell varies from 0.868 to 0.913 g/cm^3. The temperature dependence of these interfacial profiles (at constant volume) between 350 and 462.5 K is very weak; a representative profile for density at 0.890 g/cm^3 is that for the zero strain case ($\epsilon = 0$) in Figure 1. In accord with previous studies, the initial large peak in density is attributed to a propensity for short loops to form at the [001] interface in order to accommodate the large reduction in flux required by the

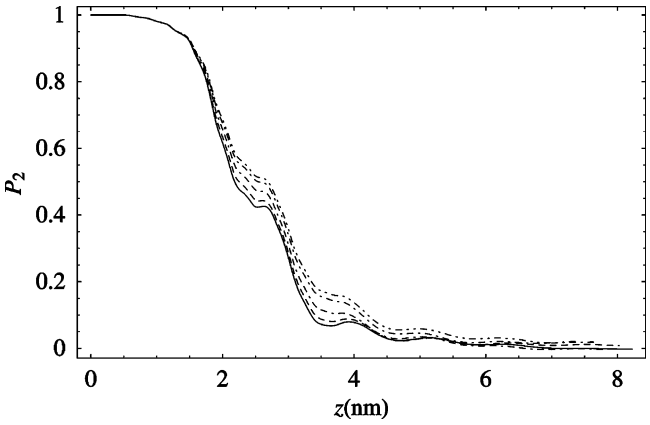

Figure 2. Order profiles for deformations normal to the [001] interface at 350 K, $\epsilon_3 \in \{-0.025, -0.013, 0.000, 0.013, 0.025\}$ in order from top curve (dot−dot−dash) to bottom curve (solid).

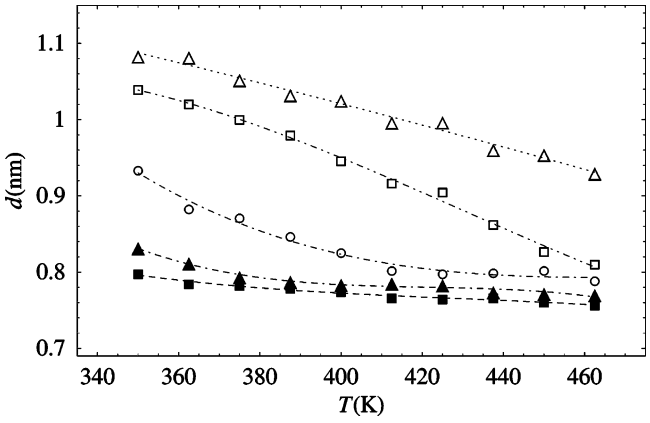

Figure 3. Interface width as a function of temperature for deformations normal to the [001] interface, $\epsilon_3 \in \{-0.025, -0.013, 0.000, 0.013, 0.025\}$ in order from top curve (dotted) to bottom curve (dashed). See text for details of calculation.

transition from crystal to amorphous structure. This peak is consistent for all densities and temperatures studied here. By contrast, the density of the amorphous material at the centerline of the simulation cell varies by as much as 8%, and the ordering of atoms into layers on the low-density side of the interface becomes more pronounced under compression.

The orientational order profile provides a measure of alignment of bond chords (vectors joining next-nearest neighbor atoms along a chain) with the normal to the crystal surface.[11] For the [001] interface, this falls off from 1.0 for a crystalline material to 0.0 for a randomly oriented material, as shown by Figure 2. Here too the profiles are qualitatively the same over the entire range of temperature. The features around 1.0 and 1.5 nm in the orientational order profiles are attributed to the presence of predominantly folded layers, as suggested by the oscillations in the density profile (Figure 1) and confirmed in previous work.[9−11] The distance over which the order function decays from 90% of its full value to 10% defines the "90−10 interfacial width". This definition results in a width of 0.94 nm at 350 K, which decreases to 0.81 nm at 462.5 K, as shown in Figure 3 for the undeformed ($\epsilon = 0$) case. The decrease in interfacial width with increasing temperature reflects the role of entropy, which favors a more amorphous interphase at higher temperatures. The interfacial thickness also decreases with decreasing density, as shown in Figure 3 for systems simulated at different levels of strain. A lower bound of about 0.8 nm is

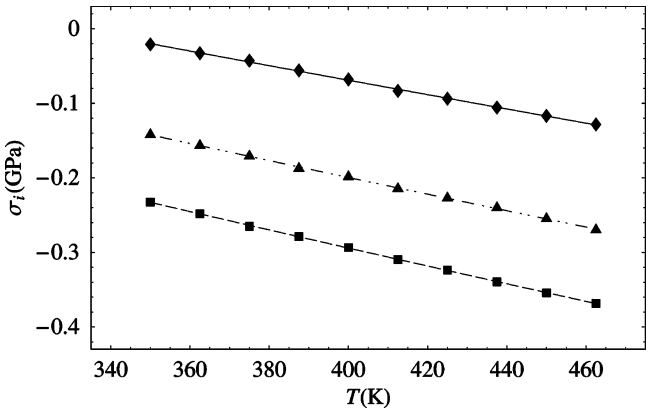

Figure 4. Three principal components of stress at the undeformed state as a function of temperature: (■) σ_1; (▲) σ_2; (♦) σ_3.

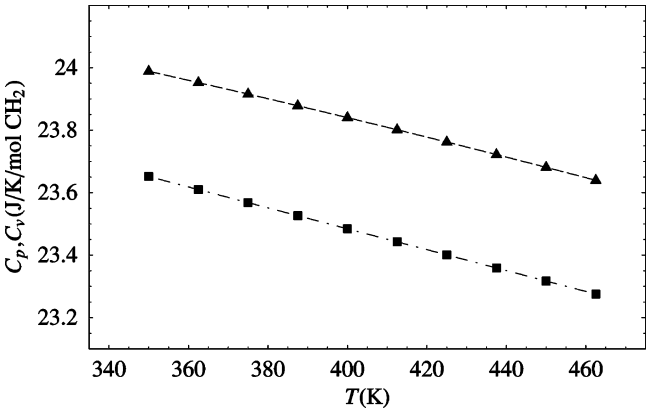

Figure 5. Isochoric (■) and isobaric (▲) heat capacities at 0.890 g/cm^3 as a function of temperature.

suggested by the data, probably due to the interface being pressed against the fixed crystal boundary of the cell. Small-angle X-ray scattering experiments by Stribeck et al.[38] indicate interfacial thicknesses in good agreement with our results. Their data also show a strong dependence of thickness on molecular weight. Solid-state high resolution ^{13}C NMR experiments by Kitamaru et al.[39] suggest an interfacial width about double our results.

3.2. Stress and Internal Energy Contribution to Stress. The principal components of the stress tensor are negative, as shown in Figure 4, indicating that the [001] interphase for the freely rotating chain described by the force field used here is under compression at these temperatures and an average density of 0.890 g/cm^3. The compressive stresses are due at least in part to the use of the amorphous phase density for polyethylene extrapolated to 300 K as a guide for the centerline of the simulation. These stresses increase in magnitude with temperature because the system is held at constant volume. The isochoric heat capacity C_v was computed from the temperature dependence of internal energy and is plotted in Figure 5. It shows a weak temperature dependence ranging from 23.7 to 23.3 J/K/mol CH_2 for temperatures from 350 to 462.5 K, respectively. C_p relates to C_v through

$$C_p = C_v + \alpha^2 K T V_m \tag{21}$$

where α is the thermal expansion coefficient, K is the bulk modulus, and V_m is the molar volume. Application of eq 21, using values of α and K described later, yields

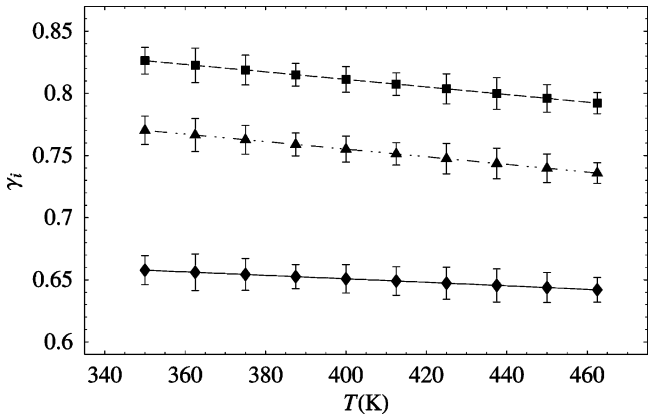

Figure 6. Grüneisen coefficients as a function of temperature: (■) γ_1; (▲) γ_2; (♦) γ_3.

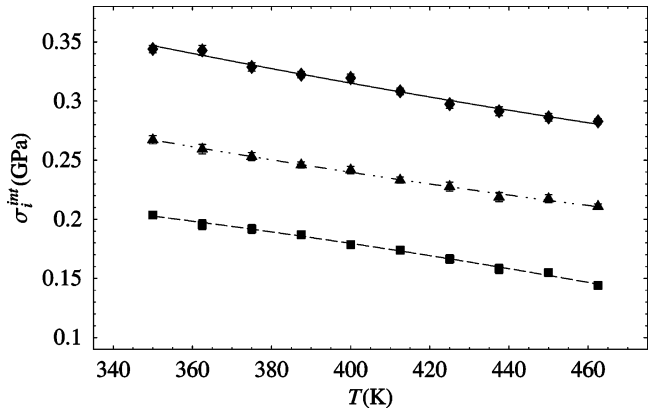

Figure 7. Three principal components of the internal stress: (■) σ_1^{int}; (▲) σ_2^{int}; (♦) σ_3^{int}.

isobaric heat capacities ranging from 24.0 to 23.6 J/K/mol CH_2 for temperatures from 350 to 462.5 K, which is about two-thirds of the values reported for polyethylene, 33.1 to 37.8 J/K/mol CH_2 for the same temperature range at atmospheric pressure.[40] The Grüneisen coefficients determined from the data of Figures 4 and 5 are calculated using eq 15 and plotted in Figure 6. The temperature dependence of the Grüneisen coefficients is due to the slight curvature in both the energy and stress curves with respect to temperature. The Grüneisen coefficients were also computed using the following equation to estimate $(\partial\sigma/\partial T)_0$,

$$\left[\frac{\partial\sigma_i}{\partial T}\right]_0 = -\frac{1}{V_0}\left[\frac{\partial S}{\partial\epsilon_i}\right]_{T,\epsilon_{k\neq i}} = \frac{1}{T}(\sigma_i - \sigma_i^{int}) \qquad (22)$$

where the first term on the right-hand side of the equation is the computed virial stress and the second term is obtained from the fit to energy at constant temperature. The internal stress is shown in Figure 7. Comparison of both calculations shows agreement to within 10%. This deviation is probably due to small nonlinearities in the elastic response for the range of strains used in this work.

3.3. Stiffness and Internal Energy Contribution to Stiffness. Elastic stiffnesses were computed from the first-order terms in the fitting function for the virial stress as a function of strain and are reported in Figure 8 and Figure 9, for diagonal (C_{ii}, $i = 1-3$) and off-diagonal (C_{ij}, $ij = 12, 23, 13$) components, respectively. The values are typically 2−4 GPa. The corresponding bulk modulus at 450 K is 3.8 GPa, which compares with

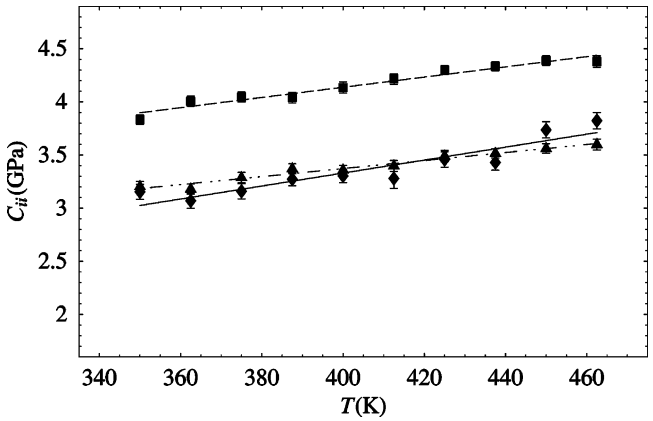

Figure 8. Diagonal contributions to the elastic stiffness matrix: (■) C_{11}; (▲) C_{22}; (♦) C_{33}.

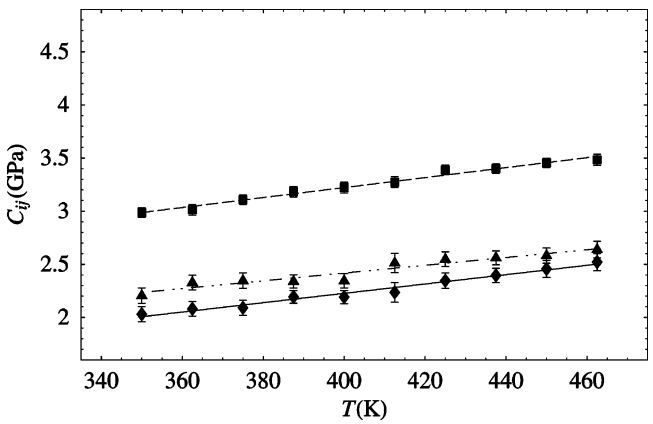

Figure 9. Off-diagonal contributions to the elastic stiffness matrix: (■) C_{12}; (▲) C_{13}; (♦) C_{23}.

a value of 3.6 GPa for a polyethylene melt under the same conditions.[41] At first glance, the increase in stiffness with temperature may appear surprising. This can be traced to the fact that these simulations were performed for a fixed reference volume, independent of temperature; thermal expansion of the reference volume has not been taken into consideration. Simulations of stable crystal phases, for example, using the method of lattice dynamics, show similar behavior; stiffness decreases with temperature at constant pressure, as reported by Lacks and Rutledge,[8] but increases with temperature when computed at constant volume, as shown in Figure 10 (using the same model as ref 8). The exception in the crystal phase, of course, is C_{33}, which decreases due to α_{33} being less than zero (also $\gamma_{33} < 0$). This temperature dependence is related to the entropic contribution to the stiffnesses

$$\frac{\partial C_{ij}}{\partial T} = \frac{\partial}{\partial\epsilon_j}\left[\frac{\partial\sigma_i}{\partial T}\right] = \frac{\partial}{\partial\epsilon_j}\left[-\frac{1}{V_0}\frac{\partial S}{\partial\epsilon_i}\right] = -\frac{1}{V_0}\frac{\partial^2 S}{\partial\epsilon_i\partial\epsilon_j} \qquad (23)$$

for fixed V_0, which can be computed independently through

$$-\frac{T}{V_0}\frac{\partial^2 S}{\partial\epsilon_i\partial\epsilon_j} = \frac{1}{V_0}\frac{\partial^2 A}{\partial\epsilon_i\partial\epsilon_j} - \frac{1}{V_0}\frac{\partial^2 E}{\partial\epsilon_i\partial\epsilon_j} = \frac{1}{V_0}\frac{\partial\sigma_i}{\partial\epsilon_j} - \frac{1}{V_0}\frac{\partial^2 E}{\partial\epsilon_i\partial\epsilon_j} \qquad (24)$$

The entropic contributions to elastic stiffness is displayed in Figure 11 for the diagonal terms. From this calculation we determine this contribution to be of the

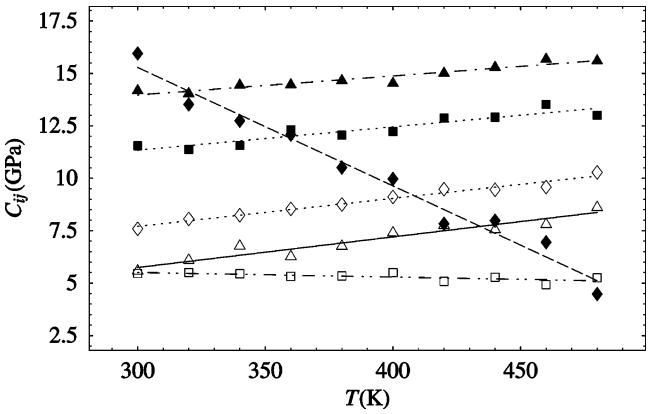

Figure 10. Lattice dynamics results for the calculation of the elastic stiffness matrix of polyethylene: (■) C_{11}; (▲) C_{22}; (♦) C_{33} minus 300 GPa; (□) C_{12}; (△) C_{13}; (◇) C_{23}.

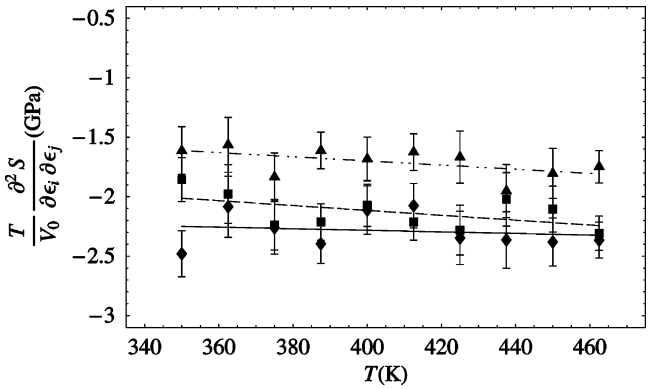

Figure 11. Diagonal contributions to the second derivative of the entropy term (text): (■) 11; (▲) 22; (♦) 33.

order of 2.0 ± 0.5 GPa; this result is in accord with earlier findings for polyethylene melts by Matheson.[36]

Finally, we can determine the thermal expansion coefficients by making use of the relation[34]

$$\alpha_i = \frac{C_v}{V_0}\sum_{j=1}^{6}\mathbf{S}_{ij}\gamma_j = -\sum_{j=1}^{6}\mathbf{S}_{ij}\left[\frac{\partial\sigma_j}{\partial T}\right]_0 \qquad (25)$$

where S_{ij} are components of the elastic compliance tensor, $\mathbf{S} = \mathbf{C}^{-1}$. Assuming that $\mathbf{C}$ is block diagonal, α_i, $i = 1-3$, can be determined from the data in Figures 6, 8, and 9. These are plotted as a function of temperature in Figure 12. The bulk thermal expansion coefficient $\alpha_{bulk} = (\alpha_1 + \alpha_2 + \alpha_3)/3$ is computed to be 1.25×10^{-4} K^{-1} at 400 K, which is lower than the corresponding value of 7.1×10^{-4} K^{-1} for a polyethylene melt at the same temperature and atmospheric pressure.[32] This difference is attributed to the presence of interfaces with the crystal phase, to the state of compression operative in the calculations and to the fact that the model is that of a freely rotating chain. The coefficients show a slight decrease with increasing temperature.

3.4. α_c Relaxation. Finally, it is possible to consider rate of strain effects on the elastic moduli, albeit in a crude fashion. The suite of Monte Carlo moves described earlier and used throughout this work was designed to sample both configuration and topology of the interphase, subject only to the simple constraints imposed

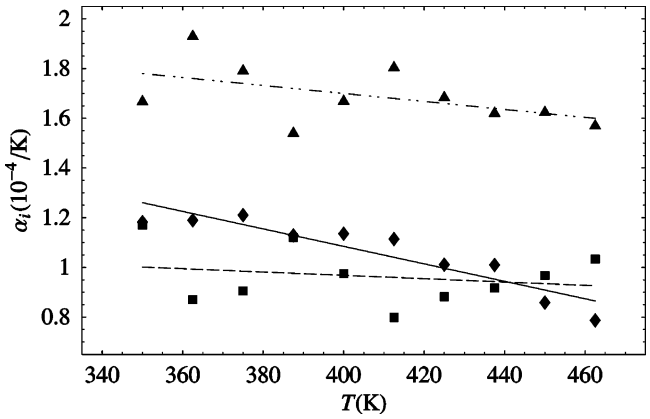

Figure 12. Thermal expansion coefficient as a function of temperature for the three directions of deformation: (■) α_1; (▲) α_2; (♦) α_3.

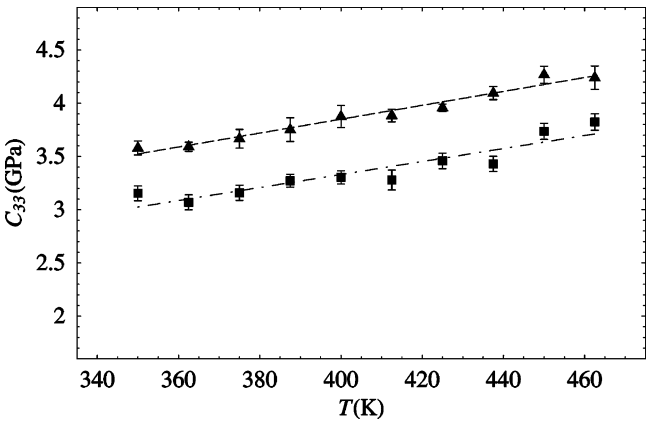

Figure 13. Elastic stiffness for deformations normal to the [001] interface for rates of deformation large and small relative to the α_c-relaxation: (■) slow deformation; (▲) fast deformation.

by eqs 1 and 2. The primary justification for topology-altering Monte Carlo moves in such a simulation is the existence of mechanisms for chain transport in the crystal, to which is attributed the α_c relaxation observed experimentally in many crystalline polymers, including polyethylene. Such mechanisms, when operative, are sufficient to alter the population of loops and bridges of various lengths. In reality, however, the α_c relaxation is an activated process, with a characteristic time constant that varies with temperature. For very slow deformation, in which the Weissenberg number $Wi \ll 1$, the relaxation rate is much larger than the deformation rate, so the deformation may be viewed as sampling a series of quasi-static states, each fully equilibrated with respect to both conformation and topology. This is the case considered implicitly up to now. However, it is also possible to construct a fully equilibrated simulation and then suppose a deformation rate that is much faster than the relaxation rate. In this case, topological equilibration would not have time to occur at each new state of strain. It is possible to approximate this situation here by turning off the end-bridging and reptation moves during simulations at finite strain, thereby allowing configurational rearrangement of the material but precluding topological rearrangements. Figure 13 shows the results for C_{33}, the elastic stiffness in the direction normal to the interfacial plane, both with and without end-bridging and reptation moves. The reference state is fully equilibrated in either case. As expected, the role of the α_c relaxation is to provide

additional mechanisms for relieving the imposed stress at a given level of strain, resulting in lower stiffness. The drop in stiffness is roughly independent of temperature.

4. Summary

We have developed a method capable of describing temperature and density dependencies of the interfacial structure and applied it to an interphase consisting of semicrystalline freely rotating polyethylene-like chains. The versatility of the method is highlighted by the array of thermoelastic properties obtained from its application. Its simplicity stems from the need for only basic *NVT* simulations. In accord with previous studies, the initial large peak in density is attributed to a propensity for short loops to form at the [001] interface in order to accommodate the large reduction in flux required by the transition from crystal to amorphous structure. The peak is found to be consistent for all studied temperatures and densities. The features around 1.0 and 1.5 nm in the orientation order profiles are attributed to the presence of predominantly folded layers, as suggested by the oscillations in the density profile and confirmed in previous work.[9−11] The decrease in interfacial width with increasing temperature reflects the role of entropy, which favors a more amorphous interphase at higher temperatures. Study of stress as a result of strain shows a system under compression at the densities chosen for simulation in this work. The entropy contribution to the stress is nonnegligible. We find the elastic stiffnesses to be temperature dependent and of the same order of magnitude as the corresponding bulk modulus of polyethylene at 450 K. All stiffnesses are lower compared to results from lattice dynamics calculations of crystalline polyethylene. As in the stress case, we find the entropic contribution to the elastic stiffnesses to be nonnegligible. The temperature dependences of thermal expansion and heat capacity are found to be negative here because no attempt has been made to correct for the rise in compressive stress with increasing temperature. We also demonstrate this method to be applicable as a crude tool in investigating of the rate of strain effect on the elastic moduli for the α_c relaxation phenomenon.

Acknowledgment. This work has been supported by the Center for Advanced Engineering Fibers and Films through the ERC program of the National Science Foundation under Award ECC-9731680 and by the MRSEC Program of the National Science Foundation under Award Number DMR-9808941.

References and Notes

(1) Al-Hussein, M.; Davies, G. R.; Ward, I. M. *J. Polym. Sci., Part B* **2000**, *38*, 755.
(2) Hageman, J. C.; Meier, R. J.; Heineman, M.; de Groot, R. A. *Macromolecules* **1997**, *30*, 5953.
(3) Montanari, B.; Ballone, P.; Jones, R. O. *J. Chem. Phys.* **1998**, *108*, 6947.
(4) Ryckaert, J. P.; Klein, M. L. *J. Chem. Phys.* **1986**, *85*, 1613.
(5) Liang, G. E.; Noid, D. W.; Sumpter, B. G.; Wunderlich, B. *Comput. Polym. Sci.* **1993**, *3*, 101.
(6) Martonak, R.; Paul, W.; Binder, K. *Comput. Phys. Commun.* **1996**, *99*, 2.
(7) Karasawa, N.; Dasgupta, S.; Goddard, W. A. *J. Phys. Chem.* **1991**, *95*, 2260.
(8) Lacks, D. J.; Rutledge, G. C. *J. Phys. Chem.* **1994**, *98*, 1222.
(9) Balijepalli, S.; Rutledge, G. C. *J. Chem. Phys.* **1998**, *109*, 6523.
(10) Balijepalli, S.; Rutledge, G. C. *Macromol. Symp.* **1998**, *133*, 71.
(11) Balijepalli, S.; Rutledge, G. C. *Comput. Theor. Polym. Sci.* **2000**, *10*, 103.
(12) Gautam, S.; Balijepalli, S.; Rutledge, G. C. *Macromolecules* **9136**, *33*, 9136.
(13) Bassett, D. C.; Hodge, A. M. *Proc. R. Soc. London* **1981**, *A377*, 25.
(14) Debenedetti, P. G. *Metastable Liquids: Concepts and Principles*; Princeton University Press: Princeton, NJ, 1996.
(15) Mansfield, M. L. *Macromolecules* **1983**, *16*, 914.
(16) Paul, W.; Yoon, D. Y.; Smith, G. D. *J. Chem. Phys.* **1995**, *103*, 1702.
(17) Bolton, K.; Bosio, S. B. M.; Hase, W. L.; Schneider, W. F.; Hass, K. C. *J. Chem. Phys. B* **1999**, *103*, 3885.
(18) Smit, B.; Karaborni, S.; Siepmann, J. I. *J. Chem. Phys.* **1995**, *102*, 2126.
(19) Yoon, D. Y.; Smith, G. D.; Matsuda, T. *J. Chem. Phys.* **1993**, *98*, 10037.
(20) Smith, G. D.; Yoon, D. Y. *J. Chem. Phys.* **1994**, *100*, 649.
(21) Kumar, S. K.; Szleifer, I.; Panagiotopoulos, A. Z. *Phys. Rev. Lett.* **1991**, *66*, 2935.
(22) Vacatello, M.; Avitabile, G.; Corradini, P.; Tuzi, A. *J. Chem. Phys.* **1980**, *73*, 548.
(23) Boyd, R. H. *Macromolecules* **1989**, *22*, 2477.
(24) Dodd, L. R.; Boone, T. D.; Theodorou, D. N. *Mol. Phys.* **1993**, *78*, 961.
(25) Mavrantzas, V. G.; Boone, T. D.; Zervopoulou, E.; Theodorou, D. N. *Macromolecules* **1999**, *32*, 5072.
(26) Pant, K. V.; Theodorou, D. N. *Macromolecules* **1995**, *28*, 7224.
(27) Uhlherr, A.; Mavrantzas, V. G.; Doxastakis, M.; Theodorou, D. N. *Macromolecules* **2001**, *34*, 8554.
(28) Kofke, D. A. *J. Chem. Phys.* **2002**, *117*, 6911.
(29) Frenkel, D.; Smit, B. *Understanding Molecular Simulation*; Academic Press: San Diego, CA, 1996.
(30) Honell, K. G.; Hall, C. K.; Dickman, R. *J. Chem. Phys.* **1987**, *87*, 664.
(31) Theodorou, D. N.; Boone, T. D.; Dodd, L. R.; Mansfield, K. F. *Makromol. Chem. Theory Simul.* **1993**, *2*, 191.
(32) Orwoll, R. A.; Flory, P. J. *J. Am. Chem. Soc.* **1967**, *89*, 6814.
(33) Rutledge, G. C. *J. Macromol. Sci. Phys.* **2002**, *B41*, 909.
(34) Nye, J. F. *Physical Properties of Crystals*; Oxford University Press: Oxford, England, 1985.
(35) Theodorou, D. N.; Suter, U. W. *Macromolecules* **1989**, *19*, 139.
(36) Matheson, R. R. *Macromolecules* **1987**, *20*, 1847.
(37) Flyvbjerg, H.; Petersen, H. G. *J. Chem. Phys.* **1989**, *91*, 461.
(38) Stribeck, N.; Alamo, R. G.; Mandelkern, L.; Zachmann, H. G. *Macromolecules* **1995**, *28*, 5029.
(39) Kitamaru, R.; Hornii, F.; Murayama, K. *Macromolecules* **1986**, *19*, 636.
(40) Gaur, U.; Wunderlich, B. *J. Phys. Chem. Ref. Data* **1981**, *10*, 119.
(41) Olabisi, O.; Simha, R. *Macromolecules* **1975**, *8*, 206.

MA0346658